Laser-Driven Micro-Pinch: A Pathway to Ultra-Intense Neutrons[*]

Putong Wang,[1,2] Xuesong Geng,[3] Guoqiang Zhang,[4,1,†] Liangliang Ji,[3,‡] and Yu-Gang Ma[5,§]

[1]*Shanghai Institute of Applied Physics, Chinese Academy of Sciences, Shanghai 201800, China*
[2]*University of Chinese Academy of Sciences, beijing 100049, China*
[3]*Laboratory of Optical Physics, Institute of Physics, Chinese Academy of Sciences, Beijing 100190, China*
[4]*Shanghai Advanced Research Institute, Chinese Academy of Sciences, Shanghai 201210, China*
[5]*Key Laboratory of Nuclear Physics and Ion-Beam Application (MOE), Institute of Modern Physics, Fudan University, Shanghai 200433, China*

Utilizing the laser-driven Z-pinch effect, we propose an approach to generate ultra-short intense MeV neutron source of femtosecond pulse duration. The self-generated magnetic field driven by a petawatt-class laser pulse compresses deuterium in a single nanowire to over 120 times of its initial density, achieving an unprecedented particle number density of 10^{25} cm^{-3}. Through full dimensional kinetic simulations including nuclear reactions, we find these Z-pinches have the capacity to generate neutron pulses of high intensity and short duration, with a peak flux reaching 10^{27} cm^{-2}s^{-1}. Such laser-driven neutron sources are beyond the capability of existing approaches and paves the way for groundbreaking applications in r-process nucleosynthesis studies and high precision Time-of-Flight neutron data measurement.

Keywords: nanowire target, Z-pinch, D-D fusion reaction, laser-plasma, neutron source

I. INTRODUCTION

Conventional neutron sources, spanning isotope, accelerator, and reactor types, have played a pivotal role in advancing diverse scientific and technological domains, including materials science and nuclear physics[1]. Spallation neutron sources, representing the forefront of this evolution, are distinguished as a novel generation of high-intensity, pulsed neutron sources. They achieve neutron flux levels near 10^{17}cm$^{-2}\cdot$s^{-1} with brief pulse widths. These attributes significantly enhance precision in Time-of-Flight (TOF) measurements, a cornerstone in nuclear reactor design and nuclear astrophysics [2–5].

Despite these advancements, the replication of high neutron flux conditions, which is crucial for understanding r-process nucleosynthesis[6], remains a formidable challenge. Integral to the cosmic formation of heavy elements, neutron star mergers is the primary site for this process[7], while the possibility of the contribution from supernovae explosions is still under debate[8]. These astrophysical events require conditions, including the intensive neutron flux ranging from 10^{22} to 10^{28}cm$^{-2}\cdot$s^{-1}, a range still elusive in laboratory settings. This gap not only hinders our comprehensive understanding of these astrophysical phenomena but also limits advancements in related fields such as nuclear physics and astrophysics. The urgency to develop new methodologies capable of achieving these extreme conditions in a controlled environment is therefore paramount.

The recent development of laser-driven high-intensity neutron sources show the potential to fill this gap due to their exceptional temporal resolution and ability to achieve highly localized neutron beams (spatial resolution) [9, 10]. These sources employ various methodologies, including photoneutron production[11, 12] (10^{21} cm$^{-2}\cdot$s^{-1}), target normal sheath acceleration (TNSA) [13, 14] (10^{24} cm$^{-2}\cdot$s^{-1}), target compression via spherical shells (NIF)[15] (10^{30} cm$^{-2}\cdot$s^{-1}). While these methods offer advancements, the neutron flux from the laser-driven Z-pinch shows the potential to surpass the current capabilities.

Z-pinch is a phenomenon where an axial current flowing through a plasma generates a magnetic field. The interaction between this magnetic field and the current creates a radial Lorentz force, which compresses the plasma radially to a small volume[16]. Fusion and x-ray researches are exploring the potential of Z-pinch devices[17–20]. Recent strides have pivoted around the augmentation of laser-driven Z-pinch mechanics from nanowire arrays[21–23], presenting notable intrigue. These nanowire arrays efficiently absorb the energy from a femtosecond petawatt laser, resulting in a high degree of ionization and intense x-ray generation[24, 25]. Additionally, ions in the array are accelerated, triggering micro-scale fusion reactions[26].

Therefore, we carried out a PIC simulation then find that a fs Petawatt laser can pinch a single nanowire to over 120 times its original density, This ultra-high density achieved through the pinch is referred to as a micro-pinch due to its tiny spatial scale and short duration. Simulations suggest that such micro-pinches can facilitate nuclear fusion reactions, leading to an intense, short-lived neutron pulse with a unprecedented flux level, 10^{27} cm^{-2}s^{-1}.

Putong Wang and Xuesong Geng contribute equally to this work

[*] This work was supported by the National Key R&D Program of China (2022YFA1602200, 2022YFA1602400), and the National Natural Science Foundation of China (No. 12235003,12388102).

[†] Corresponding author.
E-mail addresses:zhangguoqiang@sari.ac.cn

[‡] Corresponding author.
E-mail addresses:jill@siom.ac.cn

[§] Corresponding author.
E-mail addresses:mayugang@fudan.edu.cn

II. SIMULATION SETTING

To investigate the neutron generation process in a Z-pinch setup, we employ full dimensional kinetic simulations to reveal the ultra-short pinch process and the generation of neutrons using the Particle-in-Cell (PIC) code Smilei[27] code. The original nuclear reaction scheme [28, 29] has been introduced in Smilei. Specifically, the cross section for reaction $D + D \rightarrow n +^3 He$, has been integrated into the debugging version of Smilei. We have improved the debugging version, corrected and checked the nuclear reaction cross sections, using a period boundary condition in a box[30]. In addition, we have also added the nuclear reaction $D+T \rightarrow n+^4 He$ (data from [31]) in this paper to see the potential for the higher intensive neutron source.

In our simulation, the nanowire where Z-pinch is triggered is composed of deuterated polyethylene (CD_2). The particle number density of deuterium is set to $\rho = 7.8 \times 10^{22}\,\text{cm}^{-3}$. Diameters of 300 nm and 500 nm have been considered with varying wire length. The initial temperature of the particles is set at 300 Kelvin. The nanowire-target is irradiated by 400 nm wavelength circularly-polarized (CP) laser pulses of 30 fs or 60 fs FWHM duration. The dimensionless amplitude of the laser field is ranging $a_0 = 10 - 40$ ($a_0 = eE/m_e c\omega$), here e and m_e are the electron charge and mass, E is the laser electric field, ω is the laser frequency and c is the speed of light in vacuum, respectively. The focal spot size of laser should be big enough to cover the whole single nanowire. A typical focal spot size is about $5\,\mu m$, reaching a peak intensity $\sim 5 \times 10^{21}\,\text{W/cm}^2 (a_0 = 17)$. To avoid numerical heating, the size and the number of cell are adjusted dynamically, according to the volume of the nanowires. One typical cell size is set as 7.5 nm $\times$ 5 nm $\times$ 5 nm, with 27 macro-particles per cell. There are 640 $\times$ 192 $\times$ 192 cells for small-sized nanowire, corresponding to a cube $4.8\,\mu m \times 0.96\,\mu m \times 0.96\,\mu m$, which is large enough to hold the whole nanowire in. The simulation boundaries are set to open conditions for both the fields and the particles. Since the field ionization is the dominating ionization process compared with that from Coulomb collisions between particles, to save simulation time, collisional ionization is switched off. The binary collision between deuterium (tritium) is set and nuclear reaction may occur.

III. SIMULATION RESULT

When irradiated by the ultrashort, high-intensity laser pulses, the atoms inside the wire undergo field ionization. The ionization process leads to a considerable potential difference on the surface of nanowire. This potential disparity is balanced by a significant return current flowing across the nanowire's surface, maintaining quasi-neutrality. For a rough estimation, we assume electrons ionized from atoms within the nanowire are mostly distracted by the laser, corresponding to total charge of $Q = 1.3 \times 10^{-8}\,\text{C}$. The current can be calculated as $I = Q/t$, where t represents the FWHM duration of the laser, set at 60 fs. This estimated current of 2.2×10^5 A provides a starting point for further analysis of the Z-pinch dynamics.

We do the 3D simulation to illustrate this laser induced Z-pinch process. Fig. 1 shows the electrons are pulled out by a CP laser in void (negative current represented in blue), while the positive current density are the return current of electrons flowing in the opposite direction (positive current represented in red). The return current density reaches $J = 10^{15} - 10^{16}\,\text{A/cm}^2$ (a cross section of $30 \times 30\,\text{nm}^2$, $I_{max} \sim 1.4 \times 10^5$ A), consistent with the estimation. Due to the extremely high current density, the induced magnetic field around the nanowire is also significant. The 2d image in Fig. 1 illustrates the transverse magnetic field distribution in the simulation. The maximum field reaches $B_y = 1.0 \times 10^6\,\text{T}$, exceeding the incident laser field ($a_0 = 17$, $B_y = 4.6 \times 10^5\,\text{T}$). This quasi-static magnetic field exerts a $J \times B$ force on both inner and outer current (electrons) of the nanowire. The current on the inner surface of the nanowire is subjected to a force radially inward due to the generated magnetic field, whereas the forces on the outer electrons of the nanowire are opposite in direction. Hence, the nanowire is compressed inward, while electrons extracted from the nanowire are pushed outward.

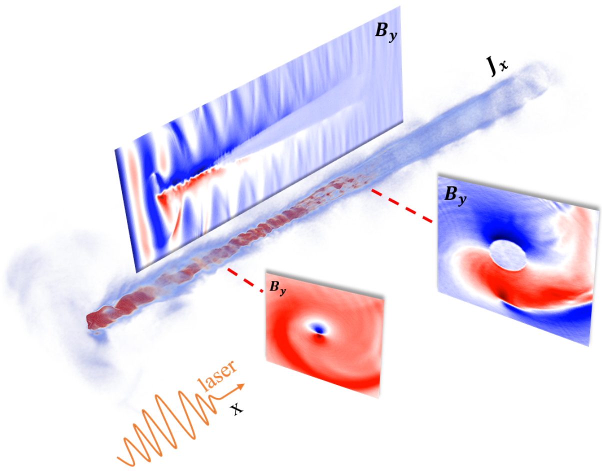

Fig. 1. The 3-D current density and 2-D magnetic fields during the pinch simulation. In the 3D image, the red color represents positive current (max $J_x = 1.4 \times 10^{16}\,\text{A/cm}^2$), while the blue color represents negative current. The 2D image illustrates the magnetic field (max $B_y = 1.0 \times 10^6\,\text{T}$. The x-positive direction aligns with the laser propagation and the axial direction of the nanowire, whereas the y and z directions correspond to the radial directions of the nanowire.

When the return electrons are pinched radially inward by Lorentz force, they induce an electric field due to charge separation. Deuterium ions are then drawn and pinched symmetrically inward from the surface by this electric field resulting in the strong radial symmetry for the kinetic energy distribution of deuterium particles within the nanowire. In our following discussion, we estimated that the temperature of deuterium in the Z-pinch is 190 keV by comparing the ratios of nuclear reaction rates. Those electrons extracted from the nanowire (that are being pushed outward) will also induce an electric

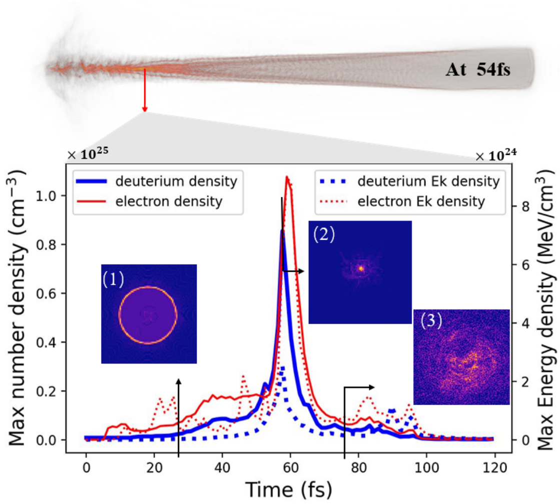

Fig. 2. The spacial and temporal profile of plasmas density and energy density. Here shows the profile at 1.2 μm from the top of the nanowire. The time-dependent variation of deuterium is depicted along the curve graph specifically at the section marked by the blue and red for electron. Dotted lines are time-dependent variation of energy density. Sub-fig(2) demonstrates the deuterium number density after compression, reaching a value around 8×10^{24} cm^{-3}.

field, drawing the surface deuterium outward and accelerating them. If it is an array target, collisions between them are also significant for nuclear reactions, because of their higher energy. Eventually the pinched-inward ions are compressed near the center creating a high density zone (Fig.2). The corresponding maximum energy density can reach the order of 1×10^{24} MeV/cm^3 (1×10^{12} J/cm^3) around 54 fs, which has two orders higher than our previous work[32].

As shown in Fig. 2, the compression happens within around $t_c = 10\,\mathrm{fs}$, and the most compression diameter is around $D = 30\,\mathrm{nm}$. The maximum density of deuterium can exceed over $\rho_m = 1\times10^{25}\,\mathrm{cm}^{-3}$, which is 120 times higher than the initial ion density. The ion (proton or deuterium) radial flux reaches around $1.0 \times 10^{34}\,\mathrm{cm}^{-2} \cdot s^{-1}$ ($\rho_m \pi D/t_c$), which is also a intense source of interest for laboratory nuclear astrophysics research[33–35]. Hence, nanowires can also serve as other nuclear reaction sources, such as $p +^{11} B \rightarrow 3\alpha$. These ions concentrate within an extremely small volume of approximately $30\times30\,\mathrm{nm}^2$, causing intense nuclear reactions, including producing neutrons. For lasers with $a_0 > 40$, the maximum density in the nanowires have a slight increase. For example, with $a_0 = 150$, there will be a maximum density of $1.8 \times 10^{25}\,\mathrm{cm}^{-3}$ on the front of wire, due to an intense axial particle acceleration and the combined effect of nanowire micro-pinch, which is long before the peak of laser pulse.When the laser intensity increases, both the magnitude of the return current density and the maximum ion density rise, but not indefinitely in our simulation. This would limit the number of nuclear reactions during the Z-pinch(Fig.4(a)). It may be caused by instability[36], such as sausage or kink instabilities in the Z-pinch effect.

Figure 3 demonstrates the number and density of nuclear

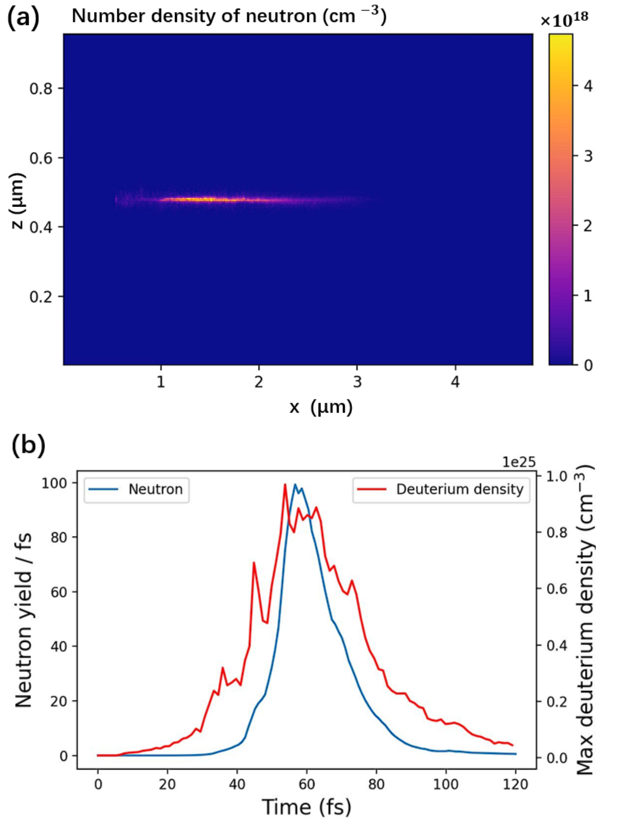

Fig. 3. (a) is Longditudinal cross section of accumulated neutron number density where the blue curve is distribution of neutron along Z-axis, which shows the spacial distribution where D-D nuclear reactions occur. The blue curve in (b) represents the number of nuclear reactions produced per femtosecond, while the red curve depicts the time evolution of deuterium maximum density. The data in the figure has been normalized. Nanowire has a diameter of 300 nm, length of 3.6 μm

reactions ($D + D \rightarrow n +^3 He$) generated by the Z-pinch. Here the propagation of the produced neutrons are not considered. It is the moment when energetic ions are colliding with each other at the densest vicinity. Due to the extremely high particle number density, it is seen that nuclear reactions primarily take place around the axis of the nanowire, as shown in Fig. 3(a). The neutron density resulting from D-D nuclear reactions is approximately on the order of $10^{18}\,\mathrm{cm}^{-3}$. The extremely short compression leads to a burst of reactions within femtoseconds, where reaction rate is over 100/fs at such a small time scale, as shown in Fig. 3(b). If suitable nuclear reactions are available, the induced reaction shows an ultra-high peak flux and ultra-short pulse duration. From the simulations, we obtain neutrons with narrow pulse width (30 fs) and a small source surface area, ($\pi 30\,\mathrm{nm} \times 3000\,\mathrm{nm} = 2.8 \times 10^5\,\mathrm{nm}^2$). The corresponding neutron (particle) flux may reach $10^{26}\,\mathrm{cm}^{-2} \cdot \mathrm{s}^{-1}$.

The figure 4(a) illustrates the relationship between laser parameters (30 fs and 60 fs, circularly polarized and linearly polarized) with the number of nuclear reactions generated by the Z-pinch. Additionally, increasing the length is efficient in

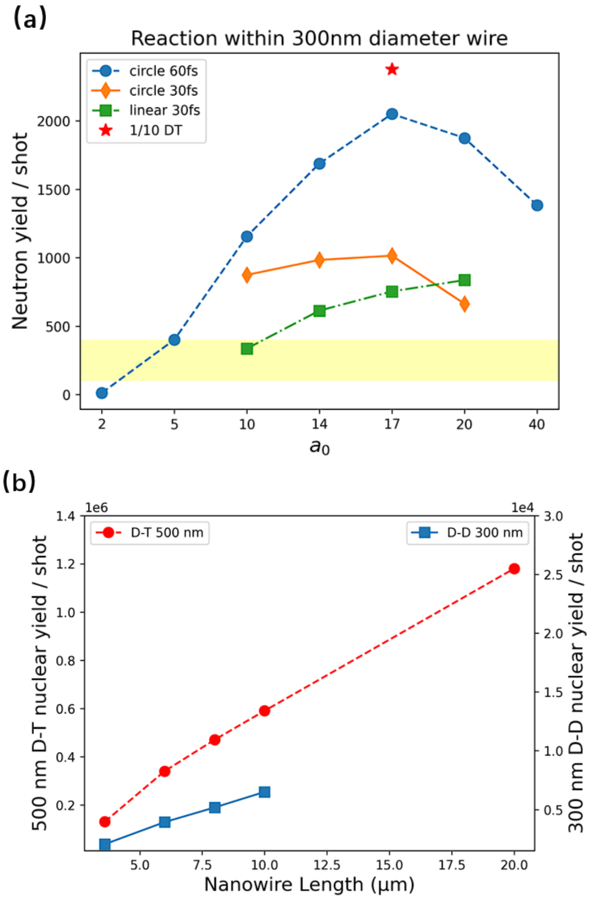

Fig. 4. (a) the relationship between the number of reaction in a nanowire with a diameter of 300 nm, length of 3.6 μm and several laser intensity. The blue circle in the diagram represents a 60 fs pulse width circularly polarized laser, while the orange and green marks represent 30 fs pulse width circularly or linearly polarized lasers. The yellow range is the approximate range of nuclear reactions that we estimate can be generated by existing Z-pinch devices under the same substance of material conditions. The red star is one-tenth of D-T reaction counts. (b) number of fusion with various length. The red circle represents D-T fusion and its yield is on the left. The blue square represents D-D fusion and its yield is on the right.

enhancing the number of nuclear reactions during the pinch phase. Diameters of nanowires also have an impact on the reaction rates. Under the same conditions, if normalized for substance of material, the efficiency of nuclear reaction generation is the highest in the diameter of 500 nm wire, followed by 300 nm. Both of these efficiencies are higher than those observed in the 200 nm and 800 nm wires.

When the D-T system is considered, the fusion yield is found more than that of D-D by over 10 times. Comparing their yield in the same system, the equivalent temperature [37] at which nuclear reactions occur in this nanowire is around 190 keV. The neutron flux could reach 10^{27} cm$^{-2}\cdot$ s^{-1} in the D-T reaction system. For the nanowire with 500 nm diameter, length with 6 μm, 8 μm and 10 μm can generate 3.4 $\times 10^5$, 4.7 $\times 10^5$ and 5.9 $\times 10^5$ neutron, respectively. It is noteworthy that this growth is almost linear with length (Due to the pulse width of the laser, the length needs to be long enough). More than 10^6 neutron could be generated within a single pulse, if the length of nanowire is increased to 20 μm, as shown in Fig4(b). Cascade reactions of D-D and D-T also occur within the system.

IV. CONCLUSION

In summary, we first conducted a study on the interaction between lasers and nanowires, with a particular focus on the Z-pinch effect. Notably, the deuterium density within the nanowire could exceed initial density by over a hundred time. We analyze the pinch density and current under different laser and nanowire parameters. It also simultaneously indicates the potential existence of stable regions in the Z-pinch effect induced by lasers. The Z-pinch effect makes laser-driven nanowires a short-time-scale, and high spatial-density environment for nuclear reactions to occur. It's suitable for use as a neutron source, which also possesses the advantages of a small spatial scale (30 nm $\times$ 30 nm), short pulse width 30 fs. This compression leads to an extremely intense and short neutron pulse. Its peak neutron flux reaches 10^{27} cm$^{-2}\cdot$s^{-1}. The high-flux nuclear reaction (neutron) sources can be utilized for research in r-process[38]. The laser can not only pinch the deuterium ions but also for the other particles as sources in nanowires. One typical example is the proton source. With radial flux around 1.0×10^{34} cm$^{-2}\cdot$s^{-1}, the proton source will provide a unique way for the two-proton capture reaction during the rp-process[39]. In addition, future studies could also utilize targets with different compositions to conduct further laboratory nuclear astrophysics research[40, 41],offering the potential to provide high-intense solutions.

[1] I. S. Anderson, C. Andreani, J. M. Carpenter, G. Festa, G. Gorini, C.-K. Loong, and R. Senesi, Physics Reports **654**, 1 (2016), publisher: Elsevier.

[2] J. Wei, H. Chen, Y. Chen, Y. Chen, Y. Chi, C. Deng, H. Dong, L. Dong, S. Fang, J. Feng, S. Fu, L. He, W. He, Y. Heng, K. Huang, X. Jia, W. Kang, X. Kong, J. Li, T. Liang, G. Lin, Z. Liu, H. Ouyang, Q. Qin, H. Qu, C. Shi, H. Sun, J. Tang, J. Tao, C. Wang, F. Wang, D. Wang, Q. Wang, S. Wang, T. Wei, J. Xi, T. Xu, Z. Xu, W. Yin, X. Yin, J. Zhang, Z. Zhang, Z. Zhang, M. Zhou, and T. Zhu, Nuclear Instruments and Methods in Physics Research Section A: Accelerators, Spectrometers, Detectors and Associated Equipment **600**, 10 (2009).

[3] R. Garoby, A. Vergara, H. Danared, I. Alonso, E. Bargallo, B. Cheymol, C. Darve, M. Eshraqi, H. Hassanzadegan, A. Jansson, I. Kittelmann, Y. Levinsen, M. Lindroos, C. Martins, Midttun, R. Miyamoto, S. Molloy, D. Phan, A. Ponton, E. Sargsyan, T. Shea, A. Sunesson, L. Tchelidze, C. Thomas,

M. Jensen, W. Hees, P. Arnold, M. Juni-Ferreira, F. Jensen, A. Lundmark, D. McGinnis, N. Gazis, J. W. II, M. Anthony, E. Pitcher, L. Coney, M. Gohran, J. Haines, R. Linander, D. Lyngh, U. Oden, H. Carling, R. Andersson, S. Birch, J. Cereijo, T. Friedrich, T. Korhonen, E. Laface, M. Mansouri-Sharifabad, A. Monera-Martinez, A. Nordt, D. Paulic, D. Piso, S. Regnell, M. Zaera-Sanz, M. Aberg, K. Breimer, K. Batkov, Y. Lee, L. Zanini, M. Kickulies, Y. Bessler, J. Ringnér, J. Jurns, A. Sadeghzadeh, P. Nilsson, M. Olsson, J.-E. Presteng, H. Carlsson, A. Polato, J. Harborn, K. Sjögreen, G. Muhrer, and F. Sordo, Physica Scripta **93**, 014001 (2017).

[4] J.-M. Xue, S. Feng, Y.-H. Chen, H. Yi, M. Xiao, P.-J. Cheng, X.-X. Li, R. Liu, Y.-W. Yang, Z.-J. Han, D.-J. Zhao, H.-Q. Wang, B.-Q. Li, J.-R. Zhao, L.-X. Tang, W. Luo, and B. Zheng, Nuclear Science and Techniques **35**, 18 (2024).

[5] G.-L. Yang, Z.-D. An, W. Jiang, X.-K. Li, W.-W. Qiu, Z.-F. Liao, Z.-Y. Zhuang, X.-P. Zhang, S.-L. Chen, C.-C. Guo, E.-X. Xiao, X. Fang, X.-X. Li, X.-R. Hu, B. Jiang, J.-C. Wang, J. Ren, W. Luo, Z.-C. Zhu, H.-Y. Lan, Z.-W. Cao, X. Ma, Y.-D. Liu, P.-S. Wang, Y. Yang, P. Su, X.-G. Deng, W.-B. He, C.-W. Ma, Y.-T. Wang, Z.-T. Dai, P.-Q. He, R.-G. Tang, T. Zhou, J. Wang, H. Yi, Y. Zhang, Y.-H. Chen, R.-R. Fan, K.-Q. Gao, Q. Li, K. Sun, Z.-X. Tan, M.-H. Gu, H.-T. Jing, J.-Y. Tang, and The CSNS Back-n Collaboration, Nuclear Science and Techniques **34**, 180 (2023).

[6] J. J. Cowan, C. Sneden, J. E. Lawler, A. Aprahamian, M. Wiescher, K. Langanke, G. Martínez-Pinedo, and F.-K. Thielemann, Rev. Mod. Phys. **93**, 015002 (2021).

[7] F.-K. Thielemann, A. Arcones, R. Käppeli, M. Liebendörfer, T. Rauscher, C. Winteler, C. Fröhlich, I. Dillmann, T. Fischer, G. Martinez-Pinedo, K. Langanke, K. Farouqi, K.-L. Kratz, I. Panov, and I. Korneev, Progress in Particle and Nuclear Physics **66**, 346 (2011), particle and Nuclear Astrophysics.

[8] E. Pian, P. D'Avanzo, S. Benetti, M. Branchesi, E. Brocato, S. Campana, E. Cappellaro, S. Covino, V. D'Elia, J. P. U. Fynbo, F. Getman, G. Ghirlanda, G. Ghisellini, A. Grado, G. Greco, J. Hjorth, C. Kouveliotou, A. Levan, L. Limatola, D. Malesani, P. A. Mazzali, A. Melandri, P. Møller, L. Nicastro, E. Palazzi, S. Piranomonte, A. Rossi, O. S. Salafia, J. Selsing, G. Stratta, M. Tanaka, N. R. Tanvir, L. Tomasella, D. Watson, S. Yang, L. Amati, L. A. Antonelli, S. Ascenzi, M. G. Bernardini, M. Boër, F. Bufano, A. Bulgarelli, M. Capaccioli, P. Casella, A. J. Castro-Tirado, E. Chassande-Mottin, R. Ciolfi, C. M. Copperwheat, M. Dadina, G. De Cesare, A. Di Paola, Y. Z. Fan, B. Gendre, G. Giuffrida, A. Giunta, L. K. Hunt, G. L. Israel, Z.-P. Jin, M. M. Kasliwal, S. Klose, M. Lisi, F. Longo, E. Maiorano, M. Mapelli, N. Masetti, L. Nava, B. Patricelli, D. Perley, A. Pescalli, T. Piran, A. Possenti, L. Pulone, M. Razzano, R. Salvaterra, P. Schipani, M. Spera, A. Stamerra, L. Stella, G. Tagliaferri, V. Testa, E. Troja, M. Turatto, S. D. Vergani, and D. Vergani, Nature **551**, 67 (2017).

[9] J. Alvarez, J. Fernández-Tobias, K. Mima, S. Nakai, S. Kar, Y. Kato, and J. Perlado, Physics Procedia **60**, 29 (2014), 3rd International Meeting of the Union for Compact Accelerator-driven Neutron Sources, UCANS III, 31 July–3 August 2012, Bilbao, Spain the 4th International Meeting of the Union for Compact Accelerator-driven Neutron Sources, UCANS IV, 23-27 September 2013, Sapporo, Hokkaido, Japan.

[10] A. Taylor, M. Dunne, S. Bennington, S. Ansell, I. Gardner, P. Norreys, T. Broome, D. Findlay, and R. Nelmes, Science **315**, 1092 (2007), https://www.science.org/doi/pdf/10.1126/science.1127185.

[11] X. Jiao, J. Shaw, T. Wang, X. Wang, H. Tsai, P. Poth, I. Pomerantz, L. Labun, T. Toncian, M. Downer, and B. Hegelich, Matter and Radiation at Extremes **2**, 296 (2017).

[12] K. W. D. Ledingham, I. Spencer, T. McCanny, R. P. Singhal, M. I. K. Santala, E. Clark, I. Watts, F. N. Beg, M. Zepf, K. Krushelnick, M. Tatarakis, A. E. Dangor, P. A. Norreys, R. Allott, D. Neely, R. J. Clark, A. C. Machacek, J. S. Wark, A. J. Cresswell, D. C. W. Sanderson, and J. Magill, Phys. Rev. Lett. **84**, 899 (2000).

[13] M. Roth, D. Jung, K. Falk, N. Guler, O. Deppert, M. Devlin, A. Favalli, J. Fernandez, D. Gautier, M. Geissel, R. Haight, C. E. Hamilton, B. M. Hegelich, R. P. Johnson, F. Merrill, G. Schaumann, K. Schoenberg, M. Schollmeier, T. Shimada, T. Taddeucci, J. L. Tybo, F. Wagner, S. A. Wender, C. H. Wilde, and G. A. Wurden, Phys. Rev. Lett. **110**, 044802 (2013).

[14] M. Günther, O. Rosmej, P. Tavana, M. Gyrdymov, A. Skobliakov, A. Kantsyrev, S. Zähter, N. Borisenko, A. Pukhov, and N. Andreev, Nature Communications **13**, 170 (2022).

[15] A. L. Kritcher, C. V. Young, H. F. Robey, C. R. Weber, A. B. Zylstra, O. A. Hurricane, D. A. Callahan, J. E. Ralph, *et al.*, Nature Physics **18**, 251.

[16] W. H. Bennett, Phys. Rev. **45**, 890 (1934).

[17] M. G. Haines, S. V. Lebedev, J. P. Chittenden, F. N. Beg, S. N. Bland, and A. E. Dangor, Physics of Plasmas **7**, 1672 (2000).

[18] M. G. Haines, Plasma Physics and Controlled Fusion **53**, 093001 (2011).

[19] V. Kantsyrev, A. Safronova, A. Esaulov, K. Williamson, I. Shrestha, F. Yilmaz, G. Osborne, M. Weller, N. Ouart, V. Shlyaptseva, L. Rudakov, A. Chuvatin, and A. Velikovich, High Energy Density Physics **5**, 115 (2009).

[20] D. D. Ryutov, M. S. Derzon, and M. K. Matzen, Rev. Mod. Phys. **72**, 167 (2000).

[21] K. K. Ostrikov, F. Beg, and A. Ng, Reviews of Modern Physics **88**, 011001 (2016), publisher: American Physical Society.

[22] V. Kaymak, A. Pukhov, V. N. Shlyaptsev, and J. J. Rocca, Phys. Rev. Lett. **117**, 035004 (2016).

[23] J. J. Rocca, M. G. Capeluto, R. C. Hollinger, S. Wang, Y. Wang, G. R. Kumar, A. D. Lad, A. Pukhov, and V. N. Shlyaptsev, Optica **11**, 437 (2024).

[24] C. Bargsten, R. Hollinger, M. G. Capeluto, V. Kaymak, A. Pukhov, S. Wang, A. Rockwood, Y. Wang, D. Keiss, R. Tommasini, R. London, J. Park, M. Busquet, M. Klapisch, V. N. Shlyaptsev, and J. J. Rocca, Science Advances **3**, e1601558 (2017).

[25] Y. Shou, D. Kong, P. Wang, Z. Mei, Z. Cao, Z. Pan, Y. Li, S. Xu, G. Qi, S. Chen, J. Zhao, Y. Zhao, C. Fu, W. Luo, G. Zhang, X. Yan, and W. Ma, Optics Express **29**, 5427 (2021), publisher: Optica Publishing Group.

[26] A. Curtis, C. Calvi, J. Tinsley, R. Hollinger, V. Kaymak, A. Pukhov, S. Wang, A. Rockwood, Y. Wang, V. N. Shlyaptsev, *et al.*, Nature communications **9**, 1077 (2018).

[27] J. Derouillat, A. Beck, F. Pérez, T. Vinci, M. Chiaramello, A. Grassi, M. Flé, G. Bouchard, I. Plotnikov, N. Aunai, J. Dargent, C. Riconda, and M. Grech, Computer Physics Communications **222**, 351 (2018).

[28] D. P. Higginson, A. Link, and A. Schmidt, Journal of Computational Physics **388**, 439 (2019).

[29] D. P. Higginson, I. Holod, and A. Link, Journal of Computational Physics **413**, 109450 (2020).

[30] Z. Zhu, J. Xu, and G.-Q. Zhang, Physical Review C **106**, 034604 (2022).

[31] *https://www.nndc.bnl.gov/* (National Nuclear Data Center).

[32] D. Kong, G. Zhang, Y. Shou, S. Xu, Z. Mei, Z. Cao, Z. Pan, P. Wang, G. Qi, Y. Lou, Z. Ma, H. Lan, W. Wang, Y. Li, P. Rubovic, M. Veselsky, A. Bonasera, J. Zhao, Y. Geng, Y. Zhao, C. Fu, W. Luo, Y. Ma, X. Yan, and W. Ma, Matter and Radiation at Extremes **7**, 064403 (2022).

[33] Z.-L. Shen and J.-J. He, Nuclear Science and Techniques **35**, 63 (2024).

[34] C. Yinji and Z. Liyong, NUCLEAR TECHNIQUES **46** (2023), 10.11889/j.0253-3219.2023.hjs.46.110501.

[35] L. Jiayinghao, L. Yunju, L. Zhihong, W. Youbao, S. Yangping, G. Bing, and L. Weiping, NUCLEAR TECHNIQUES **46** (2023), 10.11889/j.0253-3219.2023.hjs.46.080002.

[36] M. G. Haines and M. Coppins, Phys. Rev. Lett. **66**, 1462 (1991).

[37] W. Bang, M. Barbui, A. Bonasera, G. Dyer, H. J. Quevedo, K. Hagel, K. Schmidt, F. Consoli, R. De Angelis, P. Andreoli, E. Gaul, A. C. Bernstein, M. Donovan, M. Barbarino, S. Kimura, M. Mazzocco, J. Sura, J. B. Natowitz, and T. Ditmire, Phys. Rev. Lett. **111**, 055002 (2013).

[38] J. J. Cowan, C. Sneden, J. E. Lawler, A. Aprahamian, M. Wiescher, K. Langanke, G. Martínez-Pinedo, and F.-K. Thielemann, Rev. Mod. Phys. **93**, 015002 (2021).

[39] H. Schatz, A. Aprahamian, J. Görres, M. Wiescher, T. Rauscher, J. Rembges, F.-K. Thielemann, B. Pfeiffer, P. Möller, K.-L. Kratz, H. Herndl, B. Brown, and H. Rebel, Physics Reports **294**, 167 (1998).

[40] W.-P. Liu, B. Guo, Z. An, B.-Q. Cui, X. Fang, C.-B. Fu, B.-S. Gao, J.-J. He, Y.-C. Jiang, C. Lv, E.-T. Li, G.-X. Li, Y.-J. Li, Z.-H. Li, G. Lian, W.-P. Lin, Y.-H. Liu, W. Nan, W.-K. Nan, Y.-P. Shen, N. Song, J. Su, L.-T. Sun, X.-D. Tang, L.-H. Wang, S. Wang, Y.-B. Wang, D. Wu, X.-F. Xi, S.-Q. Yan, and L.-Y. Zhang, Nuclear Science and Techniques **35**, 217 (2024).

[41] W.-K. Nan, Y.-B. Wang, Y.-D. Sheng, J. Su, Y.-Q. Zhang, L.-Y. Song, Y.-P. Shen, F.-Q. Cao, C. Chen, C. Dong, Y.-J. Li, Z.-H. Li, G. Lian, W. Nan, Q. Wang, N. Song, S.-Q. Yan, S. Zeng, Q.-W. Fan, H. Zhang, M.-H. Zhu, B. Guo, and W.-P. Liu, Nuclear Science and Techniques **35**, 208 (2024).